Proceedings of the XVI National Conference on Superconductivity and Strongly Correlated Systems, Zakopane 2013

Quantum versus Classical Polarons in a Ferromagnetic CuO_3-Like Chain

K. Bieniasz[a,*] and A.M. Oleś[a,b]

[a]M. Smoluchowski Institute of Physics, Jagiellonian University, W.S. Reymonta 4, 30-059 Kraków, Poland
[b]Max-Planck-Institut für Festkörperforschung, Heisenbergstr. 1, D-70569 Stuttgart, Germany

We present an exact solution for an itinerant hole added into the oxygen orbitals of a CuO_3-like ferromagnetic chain. Using the Green function method, the quantum polarons obtained for the Heisenberg SU(2) interaction between localized Cu spins are compared with the polarons in the Ising chain. We find that magnons with large energy are favorable towards quasiparticle existence, even in the case of relatively modest electron–magnon coupling. We observe two quasiparticle states with dispersion $\sim 2t$ each, which emerge from the incoherent continuum when the exchange coupling J increases. Quantum fluctuations in the spin system modify the incoherent part of the spectrum and change the spectral function qualitatively, beyond the bands derived from the perturbation theory.

DOI: 10.12693/APhysPolA.126.A-80
PACS: 72.10.Di, 75.10.Pq, 75.50.Dd, 79.60.–i

1. Introduction

Doping charge carriers in Mott insulators frequently leads to drastic changes of the magnetic order and transport properties. For instance, in colossal magnetoresistance manganites the ferromagnetic (FM) order is accompanied by a metal–insulator transition, and appears both for hole [1] and electron [2] doping. In contrast, the antiferromagnetic (AF) interactions in CuO_2 planes is only weakened by doping while the competition between the magnetic energy and the hole dynamics leads to new phases of high temperature superconductors, such as stripe [3] or charge order [4]. A complete treatment of this problem is difficult and requires a study of the three--band model [5, 6]. Therefore, simplifications by mapping to the one-band t–J model have been performed by several authors [7–9]. The effective one-band model contains then next-nearest neighbor hopping t' [10, 11], and possibly even more distant hopping terms, which influences the value of the transition temperature T_c [12, 13].

In this paper we consider a CuO_3-like chain (depicted in Fig. 1) with FM exchange between localized Cu $S = 1/2$ spins and a single hole injected into the oxygen $2p$ orbitals. The chain structure is similar to that of a CuO_3 chain in $YBa_2Cu_3O_7$, where the superexchange is AF. It has been found that oxygen holes are then delocalized and strongly correlated [14]. Recently, excited states were investigated in AF CuO_3 chains in Sr_2CuO_3 [15] and an interesting interplay due to spin–orbital entanglement [16] was pointed out [17].

In case of FM ground state the single band model is also fundamentally different from multiband models, where charge defects are generated not in $3d$ orbitals but in $2p$ oxygen orbitals [18]. This situation resembles FM semiconductors such as EuO or EuS, where an electron with its spin aligned with the FM background moves freely, while the one with opposite spin scatters on magnon excitations which leads to rather complex many-body problem causing drastic modifications of the electronic structure [19]. In this situation as well as in the considered chain of Fig. 1, the ground state of this model is exactly known, and the spectral properties may be derived exactly [20]. Here we analyze them in detail and we show that they include both polaron-like and scattering states when the moving carrier interacts with magnons.

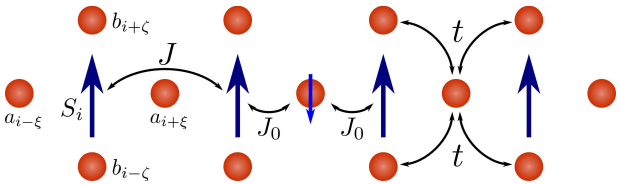

Fig. 1. Schematic representation of the CuO_3-like chain with: (i) exchange J between neighboring Cu sites (arrows) along the chain, (ii) Kondo coupling J_0 between Cu spin and the doped O spin (small arrow), and (iii) hopping t over the oxygen sites (filled circles).

2. The model

We consider a CuO_3-like FM chain, with a single $\downarrow$-spin hole doped into either of the O($2p$) states, denoted a for in-chain orbitals and b for apical orbitals (see Fig. 1). The Cu($3d_{x^2-y^2}$) states host one localized spin $S = 1/2$ each. For simplicity, all the oxygen orbitals are modeled as having s symmetry, since the difference compared to the p-d model is trivial here. Further, we reduce the number of k-states in the direction normal to the chain to just one, by taking only the binding combination of apical b states, i.e., for s symmetry $b_i = (b_{i+\zeta} + b_{i-\zeta})/\sqrt{2}$. This is done to ensure a strictly one-dimensional (1D) system and can be justified by the fact that the antibonding states do not couple to each other and thus do not appear in the kinetic term of the Hamiltonian.

*corresponding author; e-mail: krzysztof.bieniasz@uj.edu.pl

We describe the CuO_3 chain with a t–J-like model,

$$\mathcal{H} = \mathcal{T} + \mathcal{H}_{\mathrm{S}} + \mathcal{H}_{\mathrm{K}}, \tag{1}$$

where the kinetic energy $\mathcal{T}$ describes the electron hopping in the p-subspace, FM Heisenberg interaction $\mathcal{H}_{\mathrm{S}}$ couples the neighboring d states (the constant JS^2 cancels the extensive ground state energy), and a Kondo-like p-d exchange term $\mathcal{H}_{\mathrm{K}}$ which couples the two subspaces

$$\mathcal{T} = -t \sum_{i\sigma} \left[(a^{\dagger}_{i+\xi,\sigma} + a^{\dagger}_{i-\xi,\sigma}) b_{i\sigma} + \mathrm{H.c.} \right], \tag{2a}$$

$$\mathcal{H}_{\mathrm{S}} = -J \sum_{i} (\boldsymbol{S}_i \cdot \boldsymbol{S}_{i+1} - S^2), \tag{2b}$$

$$\mathcal{H}_{\mathrm{K}} = J_0 \sum_{i} \left(\boldsymbol{s}^a_{i+\xi} + \boldsymbol{s}^a_{i-\xi} + \boldsymbol{s}^b_i \right) \cdot \boldsymbol{S}_i, \tag{2c}$$

where all the energy parameters are taken as positive, i.e., $t > 0$, $J > 0$ and $J_0 > 0$. Oxygen site spin operators $\boldsymbol{s}^m_j$ are labeled by the site index j and the orbital index m serves as a reminder which of the p orbitals the site corresponds to. These operators are later expressed in standard fermionic representation for $s = 1/2$ spins. We also consider two symmetries in the $\mathcal{H}_{\mathrm{S}}$ term: (i) the SU(2) symmetry corresponding to the Heisenberg model (2b), and (ii) the Z_2 symmetry realized in the Ising model, where the scalar product in (2b) is replaced by the Ising term, $\boldsymbol{S}_i \cdot \boldsymbol{S}_{i+1} \to S^z_i S^z_{i+1}$.

To proceed, one performs a Fourier transformation (FT) and introduces a convenient matrix notation, which leads to the following representation of the Hamiltonian (2) in the p-orbital basis:

$$\mathbb{T}(k) = \begin{pmatrix} 0 & \epsilon_k \\ \epsilon^*_k & 0 \end{pmatrix}, \tag{3a}$$

$$\mathbb{V}(q) = \begin{pmatrix} \cos(q/2) & 0 \\ 0 & 1/2 \end{pmatrix}, \tag{3b}$$

where $\mathbb{V}(q)$ represents $\mathcal{H}_{\mathrm{K}}$ and $\epsilon_k = -2t\cos(k/2)$ is the dispersion relation for a bare itinerant hole. $\mathcal{H}_{\mathrm{S}}$ is treated separately by noting that in the p-orbital basis it has an identity representation, and two eigenvalues corresponding to the eigenstates spanning the magnetic subspace

$$\mathcal{H}_{\mathrm{S}} |\mathrm{FM}\rangle = 0 |\mathrm{FM}\rangle, \tag{4}$$

$$\mathcal{H}_{\mathrm{S}} S^-_q |\mathrm{FM}\rangle = \Omega_q S^-_q |\mathrm{FM}\rangle, \tag{5}$$

where

$$\Omega_q = \begin{cases} 4JS \sin^2(q/2), & \text{for Heisenberg } \mathcal{H}_{\mathrm{S}}, \\ 2JS, & \text{for Ising } \mathcal{H}_{\mathrm{S}}, \end{cases} \tag{6}$$

is the magnon dispersion relation and the FT spin operator is defined as $S^-_q = \frac{1}{N} \sum_i \mathrm{e}^{-\mathrm{i}qR_i} S^-_i$.

The problem outlined above can be solved exactly by Green's functions [18, 21], defined as the matrix representation of the resolvent operator $\mathcal{G}(\omega) = [\omega - \mathcal{H} + \mathrm{i}\eta]^{-1}$ in the state with one hole,

$$\mathbb{G}_{\mu\nu}(k,\omega) = \langle \mathrm{FM} | \mu_{k\downarrow} \mathcal{G}(\omega) \nu^{\dagger}_{k\downarrow} | \mathrm{FM} \rangle, \tag{7}$$

where $\mu, \nu \in \{a, b\}$ are indices running over the set of all orbitals taking part in the hole dynamics.

We separate the Hamiltonian 2 into the bare part $\mathcal{H}_0 = \mathcal{T} + \mathcal{H}_{\mathrm{S}}$ and the interaction $\mathcal{V} = \mathcal{H}_{\mathrm{K}}$. We define the free Green function $\mathbb{G}_0(k,\omega)$ as the Green function corresponding to $\mathcal{H}_0$, and the full Green function corresponds to the complete Hamiltonian (2). Next, we employ the Dyson expansion of the full Green function. Due to the very constrained magnetic Hilbert space consisting of just two distinct states, after performing the expansion twice the equations close, and one can express $\mathbb{G}(k,\omega)$ solely in terms of the free Green function $\mathbb{G}_0(k,\omega)$.

Due to very limited space available for this article, we do not present here any details of the rather tedious derivation. They may be found in the original paper [20], where the full derivation of the spectral function is presented. Here we give only the final result needed for the numerical analysis presented below. The full Green function can thus be expressed in the following way:

$$\mathbb{G}(k,\omega) = \Big[[\mathbb{G}_0(k,\omega)\mathbb{Q}_+(k,\omega)]^{-1} - 2J_0 S \left[\mathbb{I} - \mathbb{M}^{-1}(k,\omega) \right] \Big]^{-1}, \tag{8}$$

$$\mathbb{M}(k,\omega) = \mathbb{I} + \mathbb{G}_{cc}(k,\omega) - \mathbb{G}_{cs}(k,\omega) \times [\mathbb{I} + \mathbb{G}_{ss}(k,\omega)]^{-1} \mathbb{G}_{sc}(k,\omega), \tag{9}$$

$$\mathbb{G}_{\alpha\beta} = \frac{J_0}{N} \sum_q \mathbb{U}_{\alpha}(q) \mathbb{G}_0(k-q, \omega - \Omega_q) \times \mathbb{Q}_-(k-q, \omega - \Omega_q) \mathbb{U}_{\beta}(q), \tag{10}$$

where

$$\mathbb{U}_{\mu}(q) = \begin{cases} \mathbb{V}(q), & \mu = c, \\ \bar{\mathbb{V}}(q) = \left(\begin{smallmatrix} \sin(q/2) & 0 \\ 0 & 1/2 \end{smallmatrix} \right), & \mu = s, \end{cases} \tag{11}$$

$$\mathbb{Q}_{\pm}(k,\omega) = \left[\mathbb{I} \pm J_0 S \mathbb{V}(0) \mathbb{G}_0(k,\omega) \right]^{-1}. \tag{12}$$

Having calculated the Green function (8), we extract from it the physical information in the form of the traced spectral function,

$$A(k,\omega) = -\frac{1}{2\pi} \Im \left[\mathrm{Tr}\, \mathbb{G}(k,\omega) \right], \tag{13}$$

which is useful in the interpretation of the spectra derived from photoelectron spectroscopy experiments. In practice, throughout this article we plot $\tanh(A(k,\omega))$ to bring out the low amplitude part of the spectra.

3. Results and discussion

In our previous paper [20] we reported on the evolution of the spectral function (13) with increasing electron–magnon coupling strength, characterized by the parameter J_0. We have found that with increasing value of J_0, the spectral function changes from having two states, corresponding to the two branches of the free hole dispersion, to the five polaronic states, whose nature we explored in detail using perturbation theory [20]. We also benchmarked those results against the mean field (MF) approximation, finding that MF works well for weak coupling, while for strong coupling it highly underrates the QP binding energy, even though the quantitative results (i.e., the band shapes) are predicted surprisingly well.

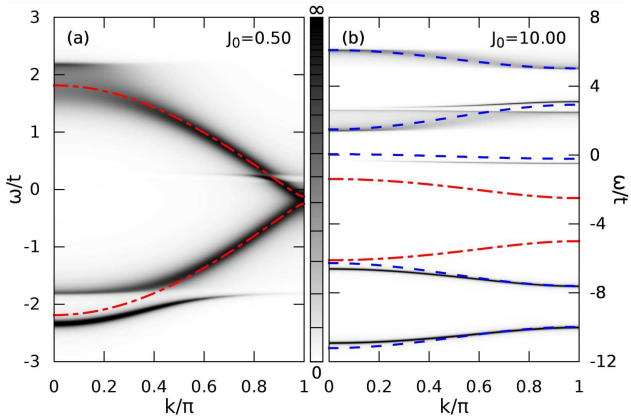

Fig. 2. Spectral functions compared with the MF solution (red dash-dotted lines) and with the perturbation expansion (blue dashed lines), as obtained for: (a) $J_0 = 0.5t$, and (b) $J_0 = 10t$. Let us note the highly nonlinear tanh-scale, with tics spaced every 0.1. Parameters: $J = 0.05t$, $\eta = 0.02t$.

Figure 2 presents a very condensed summary of our previous results [20]. Already for $J_0 = 0.5t$ one can see that new bands and gaps develop in the spectra. However, MF approximation (red dash-dotted lines) still works quite well predicting the localization of the highest density in the graph. On the other hand, for an extremely high value of $J_0 = 10t$, MF breaks down completely, while the perturbation expansion in t and J (blue dashed lines) replicates the maxima of the spectral function quite well, allowing one to identify those states as polaron-like.

In the present work we focus on the importance of the magnon energy, i.e., on establishing how the value of the parameter J influences the spectra. Figure 3 presents the evolution of the spectral function when increasing J in the range $0.05t$ to $2.0t$. The value of J_0 is set at $2.0t$, chosen so that at small J the spectrum already shows some of the polaronic features, however the bands are not yet fully developed. In fact, Fig. 3a shows this for $J = 0.05$, the value used in our previous research, which serves here as a reference state. In this graph a well developed lowest branch can be recognized, and another one just above it, still emerging from the incoherent continuum; the incoherent part is divided into two areas, separated by a small gap and well defined boundaries. Increasing J to $0.5t$ (Fig. 3b) one notices that the second band starts to mix with the incoherent spectra and a gap opens between the two branches. At $J = t$ (Fig. 3c) a new structure fades in from the incoherence, while most of the background disappears. Finally, at $J = 2t$ (Fig. 3e) the second branch is fully developed, while the incoherent part has mostly collapsed into a pair of "ghost" bands.

The spectral functions presented above have a number of noteworthy features. Firstly, compared to the strong electron–magnon coupling, even quite modest magnon energies (i.e., both J_0 and J are small and neither is the leading term) suppress the incoherent part of the spectra and aid the development of QP bands. For example,

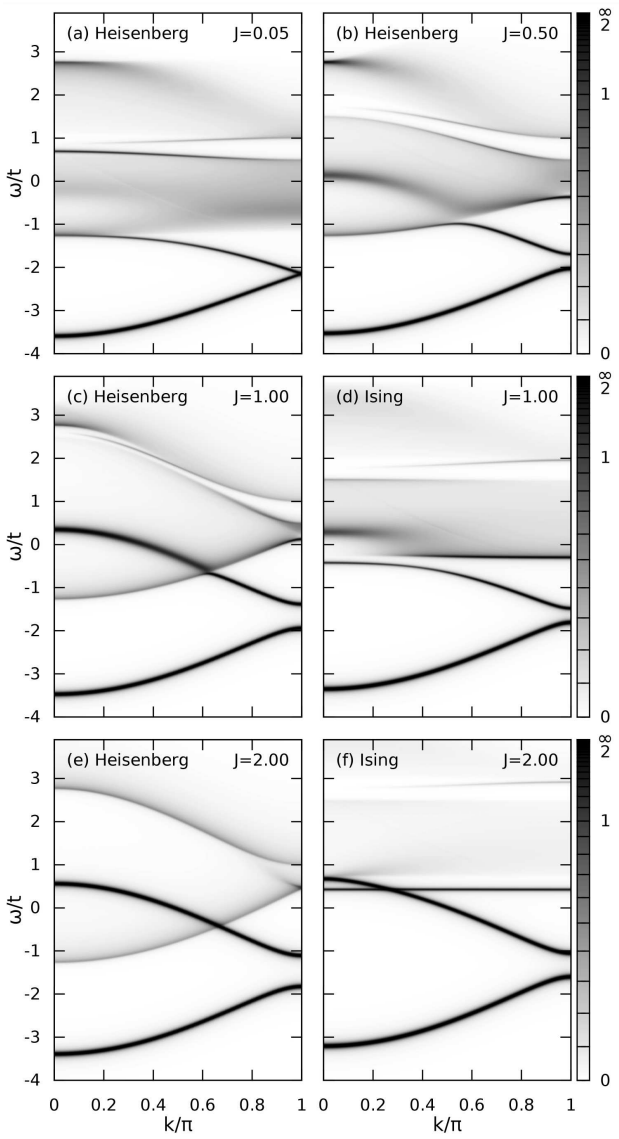

Fig. 3. Spectral function density maps for a broad range of J values obtained for: Heisenberg (a)–(c,e) and Ising (d,f) spin interaction. Let us note the highly nonlinear tanh-scale (right), with tics spaced every 0.1, used to display the features with low intensity. Parameters: $J_0 = 2t$ and $\eta = 0.02t$.

instead of three incoherent and rather complex features for $J_0 = 10t$, $J = 0.05t$ (Fig. 2b) one gets just two well defined and low amplitude bands for $J_0 = 2t$, $J = 2t$ (Fig. 3e), whose spectral weight decreases with increasing J. Those two branches correspond to the two incoherent regions mentioned before, which seems to suggest that coherence is directly linked to magnon energy.

Finally, let us consider the case of the Ising spin exchange and compare it with Heisenberg $\mathcal{H}_S$. Figure 3d, f presents the spectral functions for the Ising case, for $J = 1t$ and $J = 2t$, respectively. For very small $J = 0.05t$ (not shown), local J_0 term dominates and there is practically no difference between the Heisenberg and Ising

magnons. On the other hand, for stronger exchange interaction J the picture changes quite substantially. One notices that two QP bands exist in the Ising case for $J = 2t$ (Fig. 2f), with a slightly higher (although J-independent) binding energy and a very similar dispersion as in the Heisenberg case (Fig. 2e). However, the incoherent part of the spectrum changes far less dramatically for the Ising than it does for the Heisenberg interaction $\mathcal{H}_S$ when increasing J. Its spectral weight diminishes and the different branches move to higher energies as dictated by the value of J, but they never collapse into two states with energies increased by J_0, as seen for the Heisenberg case. The reason for this can be revealed using the perturbation theory.

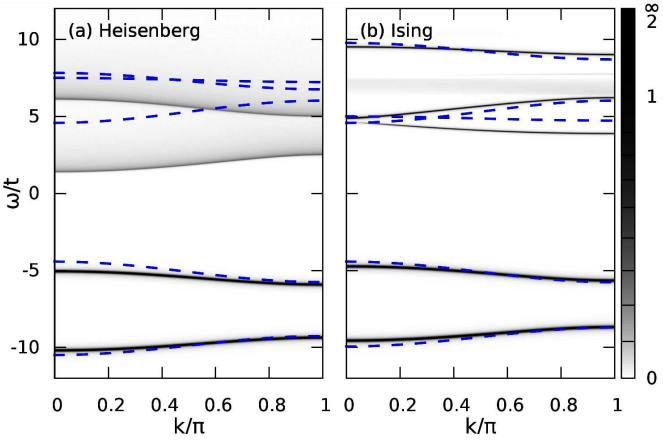

Fig. 4. Spectral weight distribution as obtained in perturbation theory (blue dashed lines) compared with the exact solution (shaded) for (a) Heisenberg, and (b) Ising exchange between localized spins. Let us note the nonlinear tanh-scale. Parameters: $J_0 = 10t$ and $J = 5t$.

Figure 4 shows the results of perturbation expansion, as outlined in [20], against the exact results for very big $J_0 = 10t$ and big $J = 5t$, for both the Heisenberg and Ising cases. This reveals some of the peculiarities in the interplay between those two parameters. First, let us note that for the Ising case the incoherent (upper) part of the spectrum is noticeably higher than for the Heisenberg case, while no such shift can be observed for the QP bands. This suggests that the quantum spin fluctuations affect only the incoherent spectra, while they are irrelevant for the QPs. Second, only two branches are seen for the Heisenberg spectrum, while there are three distinct features for the Ising case. Thus, it is clear that while the perturbation expansion works well for the Ising, it breaks down for the Heisenberg case. This breakdown depends strongly on the value of J, with the perturbation solution going gradually out of tune with the exact one with increasing J. This demonstrates a drastic redistribution of the spectral weight due to the mixing of incoherent processes.

Summarizing, we have shown that the perturbation expansion reproduces the spectra obtained in the Ising limit, while quantum fluctuations modify the incoherent part of the spectrum and generate two dispersive states. This demonstrates that quantum spin fluctuations strongly affect the incoherent part of the spectra, while they almost do not contribute to the quasiparticle part at low energy.

Acknowledgments

We thank Mona Berciu for stimulating discussions. We kindly acknowledge financial support by the Polish National Science Center (NCN) under Project No. 2012/04/A/ST3/00331.

References

[1] Y. Tokura, *Rep. Prog. Phys.* **69**, 797 (2006).

[2] A.M. Oleś, G. Khaliullin, *Phys. Rev. B* **84**, 214414 (2011).

[3] A.M. Oleś, *Acta Phys. Pol. A* **121**, 752 (2012).

[4] M. Le Tacon, A. Bosak, S.M. Souliou, G. Dellea, T. Loew, R. Heid, K.-P. Bohnen, G. Ghiringhelli, M. Krisch, B. Keimer, *Nature Phys.* **10**, 52 (2014).

[5] C.M. Varma, S. Schmitt-Rink, E. Abrahams, *Solid State Commun.* **62**, 681 (1987).

[6] A.M. Oleś, J. Zaanen, P. Fulde, *Physica B+C* **148**, 260 (1987).

[7] F.C. Zhang, T.M. Rice, *Phys. Rev. B* **37**, 3759 (1988).

[8] J. Zaanen, A.M. Oleś, *Phys. Rev. B* **37**, 9423 (1988).

[9] L.F. Feiner, *Phys. Rev. B* **48**, 16857 (1993).

[10] L.F. Feiner, J.H. Jefferson, R. Raimondi, *Phys. Rev. B* **53**, 8751 (1996).

[11] T. Tohyama, *Phys. Rev. B* **70**, 174517 (2004).

[12] L.F. Feiner, J.H. Jefferson, R. Raimondi, *Phys. Rev. Lett.* **76**, 4939 (1996).

[13] E. Pavarini, I. Dasgupta, T. Saha-Dasgupta, O. Jepsen, O.K. Andersen, *Phys. Rev. Lett.* **87**, 047003 (2007).

[14] A.M. Oleś, W. Grzelka, *Phys. Rev. B* **44**, 9531 (1991).

[15] J. Schlappa, K. Wohlfeld, K. J. Zhou, M. Mourigal, M. W. Haverkort, V. N. Strocov, L. Hozoi, C. Monney, S. Nishimoto, S. Singh, A. Revcolevschi, J.-S. Caux, L. Patthey, H.M. Ronnow, J. van den Brink, T. Schmitt *Nature* **485**, 82 (2011).

[16] A.M. Oleś, *J. Phys. Condens. Matter* **24**, 313201 (2012).

[17] K. Wohlfeld, M. Daghofer, S. Nishimoto, G. Khaliullin, J. van den Brink, *Phys. Rev. Lett.* **107**, 147201 (2011); K. Wohlfeld, S. Nishimoto, M.W. Haverkort, J. van den Brink, *Phys. Rev. B* **88**, 195138 (2013).

[18] M. Möller, G.A. Sawatzky, M. Berciu, *Phys. Rev. Lett.* **108**, 216403 (2012); *Phys. Rev. B* **86**, 075128 (2012).

[19] W. Nolting, A.M. Oleś, *Phys. Rev. B* **22**, 6184 (1980); *Phys. Rev. B* **23**, 4122 (1981).

[20] K. Bieniasz, A.M. Oleś, *Phys. Rev. B* **88**, 115132 (2013).

[21] M. Berciu, G.A. Sawatzky, *Phys. Rev. B* **79**, 195116 (2009).